

Evaluation of the performance of a $^{40}\text{Ca}^+ - ^{27}\text{Al}^+$ optical clock

Kaifeng Cui,^{1, 2, *} Sijia Chao,^{1, 2, *} Chenglong Sun,^{1, 2, 3} Shaomao Wang,^{1, 2, 3} Ping Zhang,^{1, 2, 3} Yuanfei Wei,^{1, 2, 3} Jian Cao,^{1, 2} Hualin Shu,^{1, 2} and Xueren Huang^{1, 2, †}

¹State Key Laboratory of Magnetic Resonance and Atomic and Molecular Physics Innovation Academy for Precision Measurement Science and Technology, Chinese Academy of Sciences, Wuhan 430071

²Key Laboratory of Atomic Frequency Standards, Innovation Academy for Precision Measurement Science and Technology, Chinese Academy of Sciences, Wuhan 430071

³University of the Chinese Academy of Sciences, Beijing 100049

(Dated: April 21, 2022)

We report the evaluation of the systematic shifts and the total uncertainty of an $^{27}\text{Al}^+$ optical clock sympathetically cooled by a $^{40}\text{Ca}^+$ ion. Due to its relatively low Doppler cooling limit and the suitability of its mass ratio to the $^{27}\text{Al}^+$ ion, the time dilation shift of the secular motion of our $^{40}\text{Ca}^+ - ^{27}\text{Al}^+$ clock is smaller than the shift of a $^{25}\text{Mg}^+ - ^{27}\text{Al}^+$ clock. The total systematic uncertainty of our $^{40}\text{Ca}^+ - ^{27}\text{Al}^+$ quantum logic clock has been estimated to be 7.6×10^{-18} , which was mainly limited by the uncertainty of the quadratic Zeeman shift.

INTRODUCTION

Optical clocks have been considered as promising candidates for the next definition of the International System of Units (SI) second [1, 2]. A wide range of applications in the study of fundamental physics[3] such as searching for dark matter[4, 5] or testing general relativity[6, 7], have been proposed. Single-ion optical clocks based on $^{27}\text{Al}^+$ have reached a fractional frequency uncertainty as low as 9.4×10^{-19} [8].

Unlike other single-ion optical clocks, $^{27}\text{Al}^+$ single-ion optical clocks depend on another kind of co-trapped ions to provide sympathetic cooling[9] and quantum logic readout[10] because the wavelength of the cooling laser of $^{27}\text{Al}^+$ ion is 167 nm, which is a big challenge until now. Different ion species, such as $^{25}\text{Mg}^+$ [11], $^{40}\text{Ca}^+$ [12] and $^9\text{Be}^+$ [13, 14] could be employed as the auxiliary ions. However the differences between these auxiliary ion are not obvious.

For an $^{27}\text{Al}^+$ optical clock operating at the Doppler cooling limit, uncertainties from time dilation shift due to the motion is a dominant contribution to the total clock uncertainty[11]. Research has shown that using a $^{40}\text{Ca}^+$ ion as the coolant ion, it is possible to achieve a lower Doppler cooling energy not only because $^{40}\text{Ca}^+$ has a relatively narrower Doppler cooling transition, but also because its mass ratio to $^{27}\text{Al}^+$ is appropriate[15].

In this paper, we report our recent experimental progress in the evaluation of an $^{27}\text{Al}^+$ single-ion optical clock sympathetically cooled by a $^{40}\text{Ca}^+$ ion. Our results show that the time dilation shift due to secular motion of our clock is nearly equal to half of the time dilation shift of a clock sympathetically cooled by $^{25}\text{Mg}^+$ [11], which agrees with the theoretical expectation. We also describe the clock system and present the evolution of the total systematic shifts and uncertainties of the clock transition.

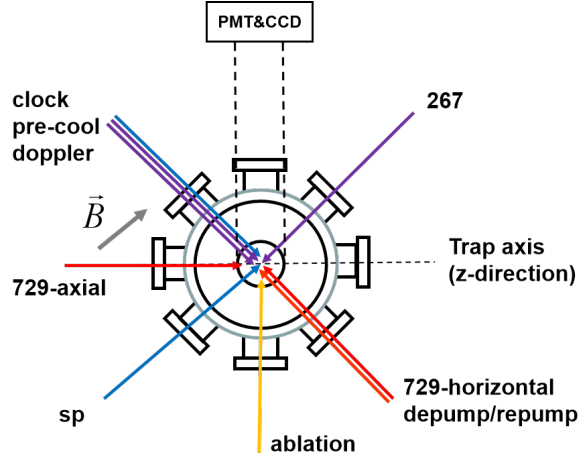


FIG. 1. Laser beamlines involved in our experiment. SP indicates the state preparation laser for the $^{40}\text{Ca}^+$ ion. 267 represents a 267 nm laser that prepares the $^{27}\text{Al}^+$ ion and helps quantum logic spectroscopy. In addition to the 729-axial and 729-horizontal beams, there is another 729-vertical beam used for the detection of EMM, which is not included in this figure.

EXPERIMENTAL SETUP

We used a linear Paul trap that is similar to that described previously [16–18]. The electrodes were made of beryllium copper to reduce the coupling capacitor. The distance between the electrodes to the ion was narrowed to 0.4 mm. A pair of end-cap electrodes were placed 8.5 mm apart along the trap axis (z-axis). With an RF drive frequency of $\nu_{RF} = 42.9$ MHz, we achieved a trap frequency of $(\omega_x, \omega_y, \omega_z) = (4.1, 4.1, 1.1)$ MHz.

An Nd: YAG laser at 1064 nm with a maximum pulse energy of 15 μJ and a pulse duration of 2 ns is used for the ablation loading of both $^{40}\text{Ca}^+$ and $^{27}\text{Al}^+$ ions from two separated metal targets. Laser cooling of the $^{40}\text{Ca}^+$ ion is implemented by a 397 nm beam that is approximately

10 MHz detuned from resonance. Another 397 nm pre-cooling beam with 120 MHz detuning is co-aligned with the Doppler cooling beam to help the ions recrystallize after collision with the background gas. A circularly polarized 397 nm laser beam (SP beam) is applied along the magnetic field direction to initialize the $^{40}\text{Ca}^+$ ion to the state $^2\text{S}_{1/2}(m = -1/2)$.

In the opposite direction, a 267 nm laser not only initialize $^{27}\text{Al}^+$ to either the state $^1\text{S}_0(m = +5/2)$ or $^1\text{S}_0(m = -5/2)$ by switching between two different polarization states, but also helps to perform the quantum logic spectroscopy, with a 729 nm laser beam along the trap axis (729-axial beam). Together with two other 729 nm beams (729-horizontal and 729-vertical), we can detect the excess micromotion in three directions.

Before each $^{27}\text{Al}^+$ clock interrogation pulse, the ions are pre-cooled for 1 ms. Then a Doppler cooling pulse of 1 ms is applied to cool the ions close to their Doppler-cooling limit. All Doppler cooling lasers are opened on during the clock interrogation pulse to ensure that the temperature of the ions remains low. A sequence of pulses then maps $^1\text{S}_0$ state of $^{27}\text{Al}^+$ ion to the dark $^2\text{D}_{5/2}(m = -1/2)$ state on $^{40}\text{Ca}^+$ through their shared motional sidebands. The readout process is repeated up to 10 times to reduce the measurement error. As described in our previous paper[16], We normally operated the clock with a interrogation time of 25 ms, corresponding to a Fourier-limited linewidth of 32 Hz.

ESTIMATION OF CLOCK TRANSITION SHIFTS

The time dilation shift due to the motion of the $^{27}\text{Al}^+$ ion has contributed to most of the uncertainty among all published works on the $^{27}\text{Al}^+$ ion optical clock. There are two types of motion for trapped ions: micromotion that is driven by the trap RF field at 42.9 MHz and harmonic-oscillator (secular) motion at the ion's normal frequencies. In both cases, as the ion moves inside an electric field, the total frequency shift needs to include a frequency-dependent term that corresponds to the Stark effect[11]:

$$\frac{\Delta v}{v} = -\frac{E_p}{mc^2} \left(1 + \frac{f}{400\text{MHz}}\right)^2 \quad (1)$$

where E_p and f are the energy and frequency of this motion respectively, and m is the mass of the $^{27}\text{Al}^+$ ion.

The secular motion energy is limited mainly by laser cooling. As we the cooling lasers are maintained on during the clock interrogation, the ions will stay close to the sympathetic Doppler cooling limit. Consider a clock ion with mass $m_2 = m$ cooled by another ion with mass m_1 , the secular motion energy of the clock ion can be written

as:

$$\begin{aligned} E_{\text{SM},i} &= \zeta_i m \omega_i^2 b_i^2 z_i^2 (\bar{n}_i + 1/2) \\ &= \text{TDS}_i (\bar{n}_i + 1/2) \end{aligned} \quad (2)$$

where TDS_i stand for the calculated value representing the time dilation shift per quantum number. $z_i = b_i z_{0,i}$ is the mode amplitude of this motion at the ground state, ω_i is the mode frequency, $z_{0,i} = \sqrt{\hbar/(2m_2\omega_i)}$, b_i is the component of the normalized eigenvector for the mode[15], and \bar{n}_i is the average motional quantum number that can be measured by comparing the amplitude of the red and blue sidebands:

$$\bar{n}_i = \frac{P_{r,i}}{P_{b,i} - P_{r,i}} \quad (3)$$

ζ_i is a factor that describes a motion driven by the trapping RF field. This motion has a frequency exactly the same as that of the driven field and exists even in an ideal Paul trap. It is called intrinsic micromotion (IMM) to be distinguished from the excess micromotion (EMM), which arises from the imperfection of the trapping potential, or phase shifts between the trap electrodes. The energy of the IMM is approximately the same as the secular energy in the transverse direction for a single ion. For two co-trapped ions, ζ_i can be expressed as[15]:

$$\zeta_{i,\text{COM}} = 1 + \frac{2\epsilon^2/\mu}{2\epsilon^2/\mu - 2\alpha - (1 - \sqrt{\mu}b_1/b_2)} \quad (4)$$

$$\zeta_{i,\text{STR}} = 1 + \frac{2\epsilon^2/\mu}{2\epsilon^2/\mu - 2\alpha - (1 + \sqrt{\mu}b_2/b_1)} \quad (5)$$

COM and STR indicate for center-of-mass mode and stretch mode, respectively. $\mu = m_2/m_1$, α and ϵ are geometric parameters for the trapping field.

One of our measurement is shown in Table I. We take several measurements in different days and take the weighted average of as the final result $-(6.9 \pm 3.1) \times 10^{-18}$. The uncertainty is given by twice the standard deviation of the measurements and is shown in the gray band in Fig. 2 (a). Our clock was operated close to the Doppler cooling limit. The secular motion energy at this cooling limit can be calculated[15]:

$$E_{i,\text{limit}} = \frac{\hbar\Gamma}{24} \frac{2(1 + 3l_i^2)}{l_i^2} \quad (6)$$

where $\Gamma = 20.4$ MHz is the natural linewidth of the $^2\text{S}_{1/2} \rightarrow ^2\text{P}_{3/2}$ transition on $^{40}\text{Ca}^+$ that is used for the Doppler cooling. l_i represent the projection of the cooling laser to i -th direction. The calculated cooling limited is listed as \bar{n}_c in Table I. This corresponding to a time dilation shift of 6.3×10^{-18} , smaller than a similar $^{27}\text{Al}^+$ clock that symmetrically cooled by $^{25}\text{Mg}^+$ [11].

In addition to the IMM, the ion may suffer from additional kinetic energy arising from the imperfection of the trapping potential. This energy E_{EMM} can be measured

TABLE I. One of the measurement results for the time-dilation shift due to secular motion. z stands for the amplitude of the motion at the ground state. \bar{n}_m represent the measured average motional quantum number. \bar{n}_c is the calculated average motional quantum number at Doppler cooling limit. TDS/quantum is the calculated time-dilation shift per quantum numbers that has included the contribution of intrinsic micromotion. For this particular measurement, the time-dilation shift is 8.34×10^{-18} . We made several measurements on different days and take the average as our final result.

Mode	\hat{x} -COM	\hat{x} -STR	\hat{y} -COM	\hat{y} -STR	\hat{z} -COM	\hat{z} -STR
Frequency(MHz)	4.00	2.84	4.03	2.84	1.17	2.10
$z(\text{nm})$	6.6	0.6	6.4	0.5	7.1	7.8
\bar{n}_m	5.2	7.0	3.0	5.7	12.8	7.5
\bar{n}_c	3.0	4.6	3.0	4.6	7.3	4.0
TDS/quantum(10^{-18})	0.747	0.004	0.757	0.003	0.030	0.118
Total TDS 10^{-18})	3.94	0.03	2.29	0.02	0.39	0.89

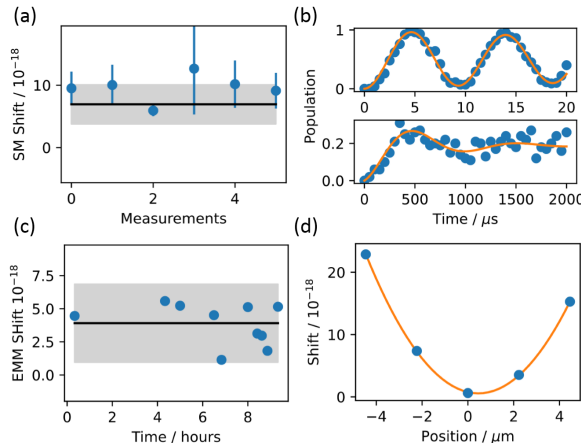


FIG. 2. Measurements of the time-dilation shift. (a) Time-dilation shift due to SM and related IMM measured over several days. We took the weighted average as the final result and estimated the uncertainty of this measurement as twice the standard deviation. (b) An example of the Rabi flopping on the carrier (top panel) and the micromotion sideband (bottom panel) on the $^{40}\text{Ca}^+$ ion driven by the 729-vertical beam. The decoherence from the magnetic field noise is the dominant error that limits the measurement of the Rabi rate on the sideband. (c) Average EMM frequency shift measured during a day. The clock is free-running without an EMM servo after the initial EMM compensation. Moreover, the order of our ion pair is not controlled. The final EMM frequency shift is $-(3.9 \pm 2.9) \times 10^{-18}$, where the uncertainty is given by twice the standard deviation and is shown in the gray band. (d) EMM shift along the trap axis. As we did not control the order of the $^{40}\text{Ca}^+$ and $^{27}\text{Al}^+$ ions, we tried to arrange the ions symmetrically around the minimal micromotion point.

through the ratio of the Rabi rate of the carrier and the EMM sideband η [19]:

$$E_{\text{EMM}} = \sum_i \frac{m\Omega_{RF}^2 \eta_i^2}{k_L^2 c^2} \quad (7)$$

i is summed over all three perpendicular directions, and k_L is the wave vector of the detection laser beam.

Our measurement of E_{EMM} is performed on the $^{40}\text{Ca}^+$ ion ($m_{\text{Ca}} = m_1$) instead of the $^{27}\text{Al}^+$ ion ($m_{\text{Al}} = m_2$).

Moreover, only have the vertical and axial beams are perpendicular to each other, while the horizontal beam is at 45° angle to the axial beam (Fig. 1). Taking this into account, the shift on $^{27}\text{Al}^+$ ion can be written as:

$$E_{\text{EMM}} = \sum_i \frac{m_1^2 \nu_{RF}^2}{m_2 \nu_1^2} (\chi_i \eta_i)^2 \quad (8)$$

where $\nu_1 \approx 411.042$ THz represents the frequency of the detection laser that excited the $^2\text{S}_{1/2} \rightarrow ^2\text{D}_{5/2}$ transition of the $^{40}\text{Ca}^+$ ion. χ_i denotes a factor that describes the projection of laser direction.

During clock operation, we started from minimizing the EMM shift by adjusting the compensation voltages, and left it free-running for the rest of the day. Therefore we continued measuring the EMM shift throughout the entire day and found the total frequency shift due to EMM by averaging those data, yielding a result of $-(3.9 \pm 2.9) \times 10^{-18}$. The uncertainty is given as twice the standard deviation, as shown in the gray band in Fig. 2 (c).

In a perfect linear Paul trap, EMM does not exist along the trap axis. However our trap is not perfect as there is a minimum axial EMM at one spatial location at a spatial location (Fig. 2 (d)). It's hard to keep the $^{27}\text{Al}^+$ ion stays at this point because random background-gas collision switched the order of our $^{40}\text{Ca}^+ - ^{27}\text{Al}^+$ pair approximately every 1000 s. We did not control the order of our ions; instead, we pushed the center of our ion pair close to this minimum point and left it free running throughout the entire day. Our measurement includes this shift due to reordering events.

The first-order Doppler shift cannot be observed for most optical clocks that work in the Lamb-Dicke regime because the motional amplitude is much smaller than the laser wavelength. However, a first-order Doppler shift may still occur when the ion itself moves in a fashion correlated with the clock laser. This movement may come from the contraction of the structure of the ion trap or additional electric field generated by the UV photoelectric effect.

We monitored this slow but long-term directional

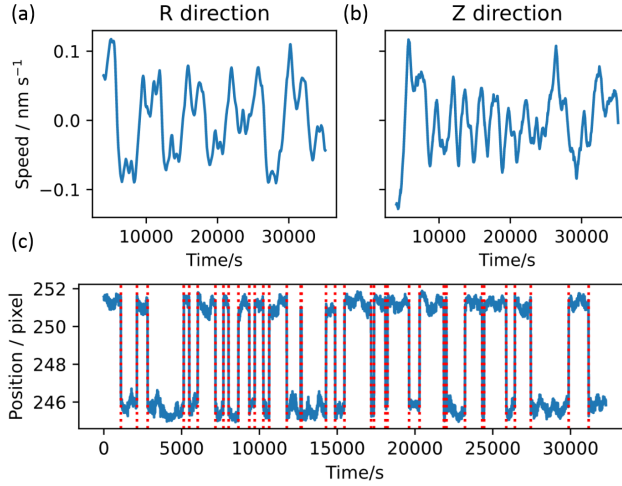


FIG. 3. (a) and (b) shows the measurement of the ion's mean velocity in one hour using the EMCCD camera, along the radial(R) direction and axial(Z) direction. The position is taken from the center of the bright spot in the camera in R direction. In the Y direction, it is the center of two possible positions due to the reorder event. (c) Part of the data that monitors the position of the bright ion along the Z-direction. The reorder event is then counted (marked as red dash lines) and used to estimate the background gas collision shift.

motion by tracking the position of the ions using an Electron-Multiplying charged-coupled device (EMCCD). Our EMCCD was positioned perpendicular to the horizontal plane (the plane of the clock laser), and the motion was detected in the laser plane. The distance between the two ions is 5.3 pixels, which can be used to calibrated the distance between two ions, as this distance is calculated to be 4.9 μm at $\omega_z = 1.12 \text{ MHz}$. The mean velocity can be calculated based on this.

The motion of ions on the EMCCD is periodic, with the same period as the temperature change period caused by the air conditioner in our laboratory. This is because the EMCCD is supported on a high platform and its supporting structure is susceptible to temperature. To eliminate this influence, we performed a moving average for one hour of data to calculate the mean velocity, as shown in Fig. 3 (a) and (b). $^{40}\text{Ca}^+ - ^{27}\text{Al}^+$ sometimes change their order along the trap axis due to the collision of the background gas with the ion pair. Therefore we took the center position of the Z-direction of the ion pair to eliminate this effect.

The velocity of ions varies within $\pm 0.1 \text{ nm/s}$. We assumed that the upper limit of the ion motion speed is 0.1 nm/s , which may still be caused by the EMCCD's support structure changes affected by temperature. This leads to a first-order Doppler shift of $(0 \pm 0.2) \times 10^{-18}$.

Although the ion trap was in an ultra-high vacuum chamber, collisions from background gas still exist causing secular motion heating and clock phase shifts. The

evaluation of the frequency shift resulting from collisions depends on the vacuum pressure p . The energy that is required by the $^{40}\text{Ca}^+ - ^{27}\text{Al}^+$ ions to change their order is given by[20]:

$$E_{reorder} = \frac{3}{4} \left(\frac{\sqrt{m}\omega_z e^2}{2\pi\epsilon_0} \right)^{2/3} \times \left(\left\{ \frac{2(\epsilon^2 + \alpha - 1)[\epsilon^2 + \mu(\alpha - 1)]}{\epsilon^2(\mu + 1) + 2\mu(\alpha - 1)} \right\}^{1/3} - 1 \right) \quad (9)$$

where e is charge of the electron. The relationship between the vacuum pressure and the reorder rate is given by:

$$\Gamma_{reorder} \lesssim \frac{1}{2} \left(\frac{p}{902 \text{nPa}} \right) \left(\frac{E_{reorder}}{1 \text{K} \times k_{\text{B}}} \right) \quad (10)$$

In our $^{27}\text{Al}^+$ clock, the reorder event can be easily observed on the EMCCD camera(3(c)) because only the position of the $^{40}\text{Ca}^+$ ion, which is the bright spot, can be seen. We measured the image for a period of 0.5 s and averaged 10 times to reduce noise. This averaging normally does not miss any reorder events as the reorder period is around 1000 s.

The reorder rate is given by $\Gamma_{reorder} = N_{reorder}/T$, where $N_{reorder}$ is the number of reorder events during time T . In our case, the reorder rate was measured to be $\Gamma_{reorder} = 0.0013 \text{ s}^{-1}$, corresponding to a vacuum pressure of 3.8 nPa. Using the empirical formula from Rosenband et. al.[13], and assuming that each collision brings a maximum phase shift of $\pi/2$, the frequency shift due to background gas collision is estimated to be 0.195 mHz, corresponding to a fractional frequency shift of 0.2×10^{-18} .

External magnetic influence is the dominant effect that causes a frequency shift of the clock transition in our $^{27}\text{Al}^+$ clock. Considering the first-order and second-order terms in the magnetic field, the two atomic resonance frequencies will be shifted[21]:

$$\nu = \nu_0 + C_1 B + C_2 \langle B^2 \rangle \quad (11)$$

where ν_0 is the unperturbed resonance frequency and C_1, C_2 are the coefficient quantifying the linear and the quadratic Zeeman shift, respectively. Here, the linear Zeeman shift is compensated by the interleaved locking of two transitions, and $\langle B^2 \rangle = \langle B \rangle^2 + B_{ac}^2$. $\langle B \rangle$ is the static (dc) component of the magnetic field measured in real time, and B_{ac}^2 is an oscillating (ac) magnetic field driven by the power line or the RF field.

$\langle B \rangle = 3.664 \times 10^{-4} \text{ T}$ can be measured with high accuracy by interleaved locking of the transitions $^2\text{S}_{1/2}(m = -1/2) \rightarrow ^2\text{D}_{5/2}(m = -5/2)$ and $^2\text{S}_{1/2}(m = +1/2) \rightarrow ^2\text{D}_{5/2}(m = +5/2)$ in the $^{40}\text{Ca}^+$ ion. For the ac component $\langle B_{ac} \rangle$, we only observe frequency jitter under 150 Hz, which results in a coherence time of 81.6 μs . This

TABLE II. BBR temperature evaluation results of the ion trap system

Components	Ω_{eff}	Value (K)	Uncertainty (K)	Uncertainty T_{eff} (K)
Blade electrode	0.457	303.87	2.90	0.110
Cap electrode	0.293	304.16	2.59	0.064
Insulation support	2.284	302.78	2.58	0.488
Compensation electrode	0.245	304.07	2.65	0.055
Stainless steel bracket	0.675	302.78	2.21	0.128
Chamber	1.264	297.97	1.43	0.169
Glass Windows	6.016	297.97	1.43	0.801
Flange	1.333	297.97	1.43	0.178

corresponds to $B_{ac} = B_{rms} = \langle B \rangle \pm 1.795 \times 10^{-7}$ T. With $C_2 = -7.9144(24) \times 10^7$ Hz/T²[21], the fractional frequency shift due to the quadratic Zeeman effect is $-(8621.0 \pm 6.2) \times 10^{-18}$.

The blackbody radiation (BBR) leads to an AC Stark shift in the clock transition. Our $^{27}\text{Al}^+$ clock is operated at room temperature (≈ 294 K), and the BBR temperature is mainly caused by the thermal radiation emitted from various components of the ion trap. We built another ion trap system with exact same configuration to achieve an accurate assessment of the BBR temperature using an infrared thermal imager. The finite element analysis method was also employed to achieve an accurate assessment of the BBR temperature[22]. The temperatures of the various components in the vacuum chamber is listed in TableII.

For the $^{27}\text{Al}^+$ ion, the effective BBR temperature can be calculated using:

$$T_{eff} = \sqrt[4]{\sum_i \frac{\Omega_{eff}}{4\pi} T_i^4} \quad (12)$$

where T_{eff} is the BBR temperature felt by the ion, and Ω_{eff} and T_i are the effective solid angle and temperature of each component of the trapped ion system, respectively. Considering the difference between the simulation and with the actual system, the uncertainty will increase slightly. Based on a conservative estimate, for the ion trap system evaluated above, we evaluated the BBR temperature as $T_{eff} = 299.6 \pm 1.4$ K. So that the clock frequency shift due to BBR is[23]:

$$\Delta\mu = -\frac{\pi k_B^4 T_{eff}^4}{60\epsilon_0 \hbar^4 c^3} (\Delta\alpha_0 \times 1.00024) \quad (13)$$

where $\Delta\alpha_0 = 4\pi\epsilon_0 \times (1.03 \pm 0.11) \times 10^{-31} m^3$ is the static differential polarizability. The corresponding BBR shift is evaluated as $-(5.3 \pm 0.6) \times 10^{-18}$.

The electric field of the optical radiation incident on the ion perturbs and shifts the line center of the ion transition. This contributes to the Stark shift[19]:

$$\Delta v_{ac} = -\frac{\Delta\alpha_{ac}(\lambda)}{2hc\epsilon_0} I \quad (14)$$

TABLE III. Fractional frequency shifts and uncertainties for the $^{27}\text{Al}^+$ quantum-logic clock

Effect	Shift(10^{-18})	Uncertainty(10^{-18})
Quad.Zeeman	-8621.0	6.2
Secular motion	-6.9	3.1
Excess micromotion	-3.9	2.9
Blackbody radiation	-5.3	0.6
Cooling laser Stark	-12.3	0.3
AOM freq. error	0	0.3
First-order Doppler	0	0.2
Background-gas collision	0	0.2
clock laser Stark	0	0.1
Total	-8627.7	7.6

where $\Delta\alpha_{ac}(\lambda)$ is the dynamic polarizability of the wavelength λ and I is the intensity of the incident light. The intensity of the clock laser was measured to be 40 nW, focused on an area of 120 μm in diameter, corresponding to an AC Stark shift $(0 \pm 0.1) \times 10^{-18}$

In additional to the clock laser itself, both the 397 nm cooling light and the 866 nm pumping light are present during clock operation. The intensity focus of those lights on the ion was 55 ± 20 nW and 91 ± 4 μW with a spot diameter of 80 μm and 150 μm , respectively. The AC Stark shifts are $-(0.042 \pm 0.015) \times 10^{-18}$ and $-(12.22 \pm 1.89) \times 10^{-18}$, respectively. The total AC Stark shift caused by the cooling lasers is $-(12.3 \pm 0.3) \times 10^{-18}$.

Phase chirp in the clock beam AOM can also contribute to a frequency shift as the optical path through the crystal changes when it switches on and off. The shift due to a phase chirp is approximately[13] $df \approx 0.2P(1-d)$ Hz, where P is the RF power drives the AOM and d is duty cycle of the AOM. We drive 1.698 mW AOM RF power to generate a 40 nW clock laser on the ion, so the shift due to this phase chirp in the clock beam AOM is $-(0 \pm 0.3) \times 10^{-18}$.

We have evaluated the fractional frequency shift and associated systematic uncertainties for our $^{27}\text{Al}^+$ clock. The results are shown in the Table III, and the total shift and associated systematic uncertainty are $-(8627.7 \pm 7.6) \times 10^{-18}$. The systematic uncertainty is limited by the quadratic Zeeman shift, which is mainly caused by the measurement uncertainty of the quadratic Zeeman

coefficient C_2 , and reducing the magnetic field $\langle B \rangle$ may lead to a significant improvement. Our measurement of the secular motion temperature is also limited by decoherence from magnetic field noise and jitter on the amplitude of the RF trapping field. In addition, controlling the order of the ions is inevitable that the uncertainty of time dilation shift due to excess micromotion can be improved.

CONCLUSION

The latest development of an $^{27}\text{Al}^+$ quantum-logic atomic clock sympathetically cooled by a $^{40}\text{Ca}^+$ ion has been reported. Owing to the relatively lower Doppler cooling limit from the $^{40}\text{Ca}^+$ ion and the suitability mass ratio to $^{27}\text{Al}^+$ ion, we achieved a smaller time-dilation shift due to secular motion than that of an $^{25}\text{Mg}^+ - ^{27}\text{Al}^+$ clock. We further studied other systematic shifts and showed that most of them have reached a level similar to that of the other $^{27}\text{Al}^+$ quantum-logic atomic clock. In conclusion, we have built an $^{27}\text{Al}^+$ quantum-logic atomic clock with a total fractional frequency shift and associated systematic uncertainty of $-(8627.7 \pm 7.6) \times 10^{-18}$.

We thank M. Zhan for the helpful suggestion. This work was supported by the National Development Project for Major Scientific Research Facility (Grant No.ZDYZ2012-2), the National Key R&D Program of China (Grant No.2017YFA0304401), the Strategic Priority Research Program of the Chinese Academy of Sciences (Grant No.XDB21030100), the Technical Innovation Program of Hubei Province (Grant No.2018AAA045) and the National Natural Science Foundation of China (Grant No.11904387).

- [6] C. W. Chou, D. B. Hume, T. Rosenband, and D. J. Wineland, *Science* **329**, 1630 (2010).
- [7] M. Takamoto, I. Ushijima, N. Ohmae, T. Yahagi, K. Kokado, H. Shinkai, and H. Katori, *Nat. Photonics* **14**, 411 (2020).
- [8] S. M. Brewer, J.-S. Chen, A. M. Hankin, E. R. Clements, C. W. Chou, D. J. Wineland, D. B. Hume, and D. R. Leibrandt, *Phys. Rev. Lett.* **123**, 033201 (2019).
- [9] D. Kielpinski, B. E. King, C. J. Myatt, C. A. Sackett, Q. A. Turchette, W. M. Itano, C. Monroe, D. J. Wineland, and W. H. Zurek, *Phys. Rev. A* **61**, 032310 (2000).
- [10] P. O. Schmidt, T. Rosenband, C. Langer, W. M. Itano, J. C. Bergquist, and D. J. Wineland, *Science* **309**, 749 (2005).
- [11] C. W. Chou, D. B. Hume, J. C. J. Koelemeij, D. J. Wineland, and T. Rosenband, *Phys. Rev. Lett.* **104**, 070802 (2010).
- [12] M. Guggemos, D. Heinrich, O. A. Herrera-Sancho, R. Blatt, and C. F. Roos, *New J. Phys.* **17** (2015).
- [13] T. Rosenband, D. B. Hume, P. O. Schmidt, C. W. Chou, A. Brusch, L. Lorini, W. H. Oskay, R. E. Drullinger, T. M. Fortier, J. E. Stalnaker, S. A. Diddams, W. C. Swann, N. R. Newbury, W. M. Itano, D. J. Wineland, and J. C. Bergquist, *Science* **319**, 1808 (2008).
- [14] T. Rosenband, P. O. Schmidt, D. B. Hume, W. M. Itano, T. M. Fortier, J. E. Stalnaker, K. Kim, S. A. Diddams, J. C. J. Koelemeij, J. C. Bergquist, and D. J. Wineland, *Phys. Rev. Lett.* **98**, 220801 (2007).
- [15] J. B. Wubbena, S. Amairi, O. Mandel, and P. O. Schmidt, *Phys. Rev. A* **85**, 043412 (2012).
- [16] S.-J. Chao, K.-F. Cui, S.-M. Wang, J. Cao, H.-L. Shu, and X.-R. Huang, *Chinese Phys. Lett.* **36**, 120601 (2019).
- [17] J.-J. Shang, K.-F. Cui, J. Cao, S.-M. Wang, S.-J. Chao, H.-L. Shu, and X.-R. Huang, *Chin. Phys. Lett.* **33**, 103701 (2016).
- [18] K.-F. Cui, J.-J. Shang, S.-J. Chao, S.-M. Wang, J.-b. Yuan, P. Zhang, J. Cao, H.-L. Shu, and X.-R. Huang, *J. Phys. B: At. Mol. Opt. Phys.* **51**, 045502 (2018).
- [19] D. J. Berkeland, J. D. Miller, J. C. Bergquist, W. M. Itano, and D. J. Wineland, *J Appl Phys* **83**, 9 (1998).
- [20] A. M. Hankin, E. R. Clements, Y. Huang, S. M. Brewer, J.-S. Chen, C. W. Chou, D. B. Hume, and D. R. Leibrandt, *Phys. Rev. A* **100**, 033419 (2019).
- [21] S. M. Brewer, J.-S. Chen, K. Belyov, A. M. Hankin, E. R. Clements, C. W. Chou, W. F. McGrew, X. Zhang, R. J. Fasano, D. Nicolodi, H. Leopardi, T. M. Fortier, S. A. Diddams, A. D. Ludlow, D. J. Wineland, D. R. Leibrandt, and D. B. Hume, *Phys. Rev. A* **100**, 013409 (2019).
- [22] P. Zhang, J. Cao, H.-L. Shu, J.-B. Yuan, J.-J. Shang, K.-F. Cui, S.-J. Chao, S.-M. Wang, D.-X. Liu, and X.-R. Huang, *J. Phys. B: At. Mol. Opt. Phys.* **50**, 015002 (2016).
- [23] T. Rosenband, W. M. Itano, P. O. Schmidt, D. B. Hume, J. C. J. Koelemeij, J. C. Bergquist, and D. J. Wineland, *ArXiv* 061125 (2006).

* These two authors contributed equally

† hxueren@apm.ac.cn

- [1] F. Riehle, *Comptes Rendus Physique The Measurement of Time / La Mesure Du Temps*, **16**, 506 (2015).
- [2] J. Lodewyck, *Metrologia* **56**, 055009 (2019).
- [3] M. S. Safranova, D. Budker, D. DeMille, D. F. J. Kimball, A. Derevianko, and C. W. Clark, *Rev. Mod. Phys.* **90**, 025008 (2018).
- [4] C. J. Kennedy, E. Oelker, J. M. Robinson, T. Bothwell, D. Kedar, W. R. Milner, G. E. Marti, A. Derevianko, and J. Ye, *Phys. Rev. Lett.* **125**, 201302 (2020).
- [5] P. Wcisło, P. Ablewski, K. Belyov, S. Bilicki, M. Bober, R. Brown, R. Fasano, R. Ciuryło, H. Hachisu, T. Ido, J. Lodewyck, A. Ludlow, W. McGrew, P. Morzyński, D. Nicolodi, M. Schioppo, M. Sekido, R. L. Targat, P. Wolf, X. Zhang, B. Zjawin, and M. Zawada, *Sci. Adv.* **4**, eaau4869 (2018).